CrossMark

Effect of Substrates Temperatures on the Spreading Behavior of Plasma-Sprayed Ni and Ni-20 wt.% Cr Splats

Yongang Zhang, Margaret Hyland, Anh Tuyet Tran, and Steven Matthews

(Submitted May 8, 2015; in revised form June 21, 2015)

In the formation of plasma-sprayed splats, the spreading behavior of molten droplets is essential for forming desirable lamella with good adhesion to the substrate. To understand the effect of the active element chromium on droplet spreading, pure Ni and Ni-20 wt.% (Ni20Cr) alloyed powders were plasma sprayed on mirror-polished 304 stainless steel substrates heated to different temperatures (below 200 °C). The substrate heating resulted in very little change in the surface roughness. However, there was a measureable change in the surface chemistry of the outermost few nanometers, which became increasingly enriched in Fe at higher temperatures. The splat morphologies were characterized and the transition temperatures were estimated. The results show that the transition from splashed to disk splats was not solely dependent on the temperature of the substrate. In some cases, some splashing still occurred to a measureable extent even at relatively high substrate temperatures, even above temperatures at which adsorbates (moisture) were totally removed from the surface. The splashing behavior could be correlated to a combination of the change in the surface chemistry of the substrate and the presence of active elements in the coating materials.

Keywords	active elements, plasma spray, splat morphology, spreading behavior, transition temperature

1. Introduction

In plasma spraying, powder particles are injected into a plasma stream where they are heated and accelerated towards the substrate. Upon impact, heated particles rapidly form single splats and build up on one another to form the coating. It is well established that these particles may undergo a transition from splashed shapes to disk shapes when the substrate is heated to a critical temperature (Ref 1, 2). This critical temperature is defined as the transition temperature, above which more than 50% of splats are disk shaped. This complicated phenomenon is related to the droplet impact conditions, surface properties of the substrate (roughness and chemistry), and interactions along the splat-substrate interface (contact conditions). In consideration of one single splat, good interfacial contact with the substrate and less delamination are required to achieve desirable coating properties, which

is also dependent on the splat morphology (Ref 3, 4). A number of studies have been conducted to investigate the splashing behavior of plasma-sprayed splats, but the cause of this phenomenon is not fully understood (even under the same spraying conditions). The presence of adsorbates (Ref 5) and moisture (Ref 6, 7) on the substrate surface could form a gas layer along the substrate-droplet interface during droplet spreading. This layer could increase the thermal contact resistance between the droplet and substrate, resulting in poor heat conduction from the droplet towards the substrate. As a result, a part of the liquid droplet may either ''over spread'' on the substrate or jet away from the main splat body, forming fragments and splashed fingers, respectively. It is supposed that preheating substrates to 150 °C can efficiently remove surface moisture and promote disk splats (Ref 8). During thermal treatment, the substrate surface roughness changes and can influence the splat morphology change. Researchers have correlated the changes in skewness of the substrate, from negative to positive, to more disk splats, which was attributed to the improved wettability of droplets (Ref 9, 10). However as R_a increases, splat splashing may occur due to the increased friction along the substrate-droplet interface and decreased cooling rates of the droplet may occur (Ref 11).

Furthermore, the wetting behavior of droplets on a substrate surface is of interest because it will influence the flattening dynamics of the droplets and the heat transfer from the droplets to substrate (Ref 12). In the measurements of static wetting characteristics of copper (Cu) droplets onto alumina, after alloying with chromium (Cr), the segregation of Cr_2O_3 to the droplet-alumina substrate interface was believed to significantly improve the wetta-

---

Yongang Zhang, Margaret Hyland, Anh Tuyet Tran, and **Steven Matthews**, Department of Chemical and Materials Engineering, The University of Auckland, Auckland, New Zealand. Contact e-mail: yzha711@aucklanduni.ac.nz.

bility of Cu (Ref 13). Similarly, for Cu droplets on both zirconia (Ref 14) and alumina (Ref 15), the addition of Cr was observed to reduce the contact angles. The segregation of chromium oxides along droplet-substrate interface was thought to decrease the solid-liquid interfacial energy and enhance the droplet wettability. In the case of thermally sprayed droplets, when a splat does not effectively wet the substrate, it is possible that splat splashing and poor interfacial contact are generated. In addition, material splashing can be reduced and the formation of disk splats is promoted with improved droplet wettability. Therefore, enhanced wettability is also likely to be linked with a lower transition temperature, meaning that disk splats can be more easily formed. It has been observed that when Nickel (Ni) is alloyed with Cr, the transition temperature of Ni-Cr splats is significantly reduced, about 170 °C smaller than pure Ni (Ref 2). The decreased transition temperature is probably related to the improved wettability with the Cr additive. So it is interesting to investigate the effect of active elements on splat spreading.

In this paper, the effect of alloying the active element Cr with Ni on the splat formation and morphology change in plasma spraying is studied. In addition, the difference in splat spreading behavior between Ni and Ni20Cr powders on 304 stainless steel substrates preheated at different temperatures is studied.

2. Experimental Procedures

2.1 Materials

Ni (Metco 56C-NS) and Ni20Cr (Metco 5640NS) powders with a sieved size of 45-63 μm (mean size $D_0 = 54$ μm) were selected as spray powders and the mirror-polished 304 stainless steel was used as substrates (size 30 mm length × 30 mm width × 2 mm thickness). Figure 1 shows the morphology of Ni and Ni20Cr powders. The sieved Ni and Ni20Cr powders (Fig. 1a and b) showed a narrow size distribution. Some irregular feedstock particles of Ni were found because this type of powder was manufactured through precipitation. Even though the majority of Ni20Cr particles showed spherical shapes, some small nodules could still be observed attached to the outer surface of some particles. In addition, the particle size distribution was analyzed by the laser particle size analyzer (Mastersizer 2000, Malvern, UK) and ImageJ software (National Institutes of Health, Washington, DC) for the obtained images.

2.2 Splats Collection

The powders were sprayed onto the substrates using a 3 MB plasma gun (Sulzer Metco). The plasma spraying parameters are shown in Table 1.

Figure 2 shows the plasma spray setup to collect single splats on different heated substrates. In order to collect single splats, a stainless steel shielding plate with 8 mm diameter holes was installed in front of the substrate surface at a distance of 20 mm. Six samples were mounted
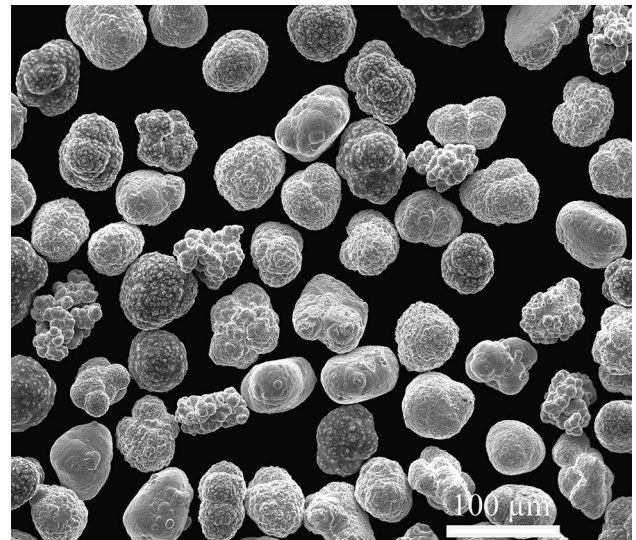
(a)
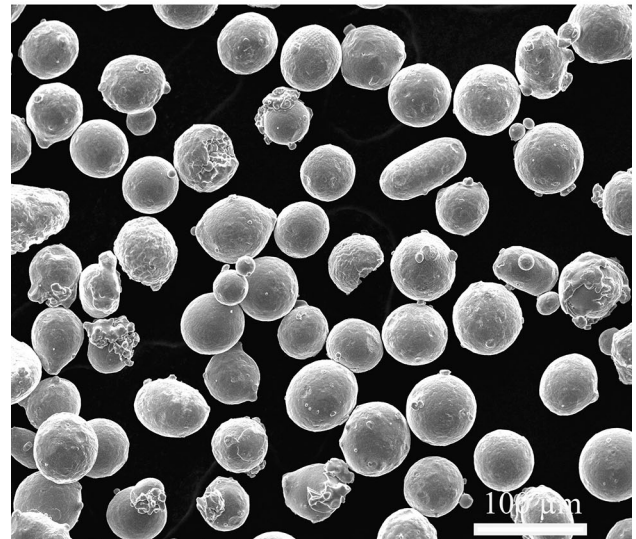
(b)

Fig. 1 The powder morphologies of (a) Ni and (b) Ni20Cr

Table 1 Plasma spraying parameters

Parameters	Value
Current, A	550
Voltage, V	65
Primary gas, L/min, LPM	Argon: 46
Secondary gas, LPM	Hydrogen: 6.4
Carrier gas, LPM	Argon: 3
Feed rate, g/min	1.4
Standoff distance, mm	100
Robot speed, m/s	0.4

onto electric resistance heaters (Eurotherm) to reach the desired temperatures, room temperature (RT), 100 °C, 125 °C, 150 °C, 175 °C, and 200 °C. To keep the temperatures consistent, the temperature of the heaters was controlled by a PID controller (Eurotherm MODBUS
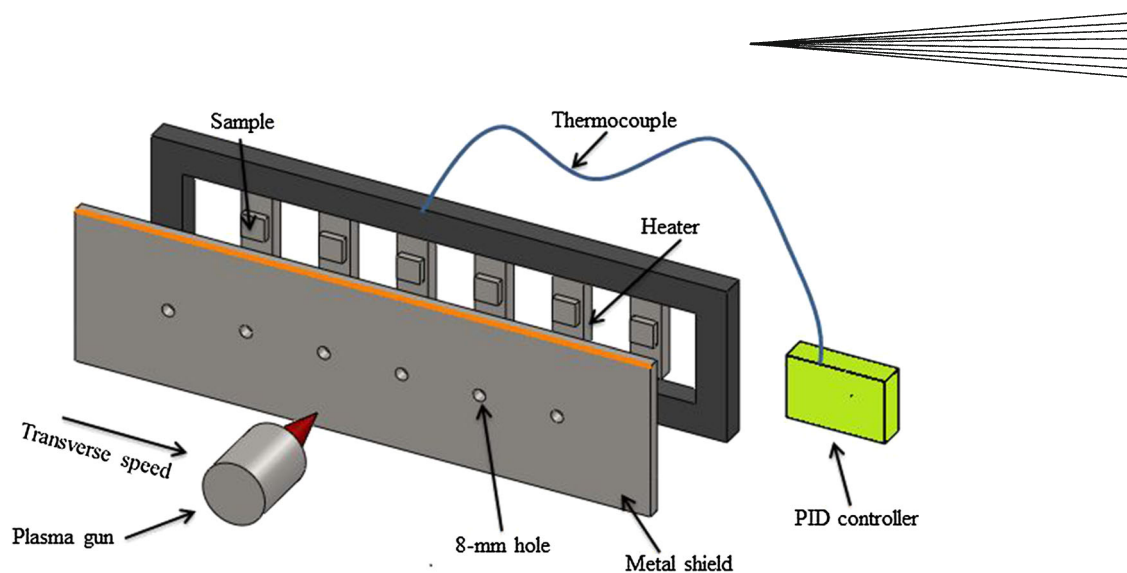
Fig. 2 Experimental setup for plasma spraying

Mini8). Prior to the spray trials, the substrate temperatures were calibrated to ensure the substrate surface reach the desirable temperatures. During the calibration, a K-type thermocouple was used to measure the substrate temperatures both at the surface center and the edge. It was found there was a difference of 10 °C between the center and the edge. However, in order to keep the surface center intact, the temperature of the substrate surface corner was checked before splats collection to confirm the temperature of the substrate surface center. After keeping the substrates on the heaters for 30 min to remove condensates from the substrate surface, the plasma spray gun passed across substrate surface in one pass. Because the shielding plate could block the high temperature plasma stream, it was assumed that the surface temperature of substrates was kept stable before particle impact (Ref 16).

2.3 Characterization of Splat Morphology

The splat morphology was observed using environmental scanning electron microscopy (FEI Quanta 200) and optical microscopy (OLYMPUS BX60M). The images were processed by ImageJ software. In this study, for each temperature parameter, around 100 splats were analyzed to obtain the average splat diameter and standard deviation.

2.4 Characterization of Substrate Surface Properties

The surface chemistry and surface roughness of the substrates were analyzed by x-ray photoelectron spectroscopy (XPS, the Kratos Axis DLD) and Scanning probe microscopy (SPM). All substrates were heated under the same conditions as used in the plasma spraying trials. Afterwards, the substrates were kept in a desiccator to avoid moisture re-adsorption and analyzed within 1 h. For XPS analysis, both wide scans and high-resolution narrow scans were performed to precisely obtain the surface composition and chemical compounds using an Al Kα x-ray source. The curve fitting was processed through CasaXPS software and all the binding energies were cal-
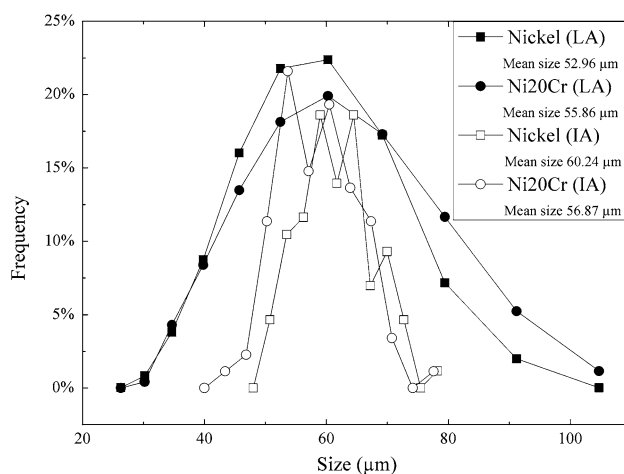

Fig. 3 The particle size distribution of Ni and Ni20Cr powders (LA—laser particle analysis, IA—image analysis)

ibrated with respect to C 1s (285.0 eV). SPM analysis was performed in a TI-950 TriboIndenter instrument (Hysitron Inc., USA) using a cube corner tip (radius ~100 nm) with a scan area of $50 \times 50 \ \mu m^2$. The surface roughness tests were repeated four times.

3. Results

3.1 Particle Size Distribution

The measured distribution and mean sizes of Ni and Ni20Cr powders are shown in Fig. 3. It was found that for these two powders, most of the particles fell in the range of 40-70 μm even though a small number of particles were out of this range. However, the mean particle size ($D_0 = 54$ μm) can still be used to estimate the splat spreading behavior such as the flattening ratios (Ref 17) and the central flat area ratios.

Table 2 Surface roughness, R_a, R_q, and S_k of substrates at different temperatures

	RT	150 °C	200 °C
R_a, nm	3.95 ± 1.11	3.17 ± 0.41	4.78 ± 0.51
R_q, nm	4.94 ± 1.40	3.97 ± 0.45	5.60 ± 0.53
S_k	0.24 ± 0.31	0.15 ± 0.17	0.32 ± 0.13

Table 3 Changes of surface composition (relative atom percent) on heated and unheated substrate surfaces

	O	C	Cr	Fe	Mn
RT	31	65	2	1	<1
150 °C	47	40	2	10	<1
200 °C	53	30	<1	15	<1

3.2 The Substrate Surface Chemistry and Roughness

As discussed in section 1, the substrate surface roughness plays an important role in determining the spreading dynamics, wettability, and solidifying behavior of droplets. Hence, the surface topology of the mirror-polished substrates as estimated by the average surface roughness (R_a), root mean square roughness (R_q), and skewness (S_k) is summarized in Table 2. These three surface roughness parameters are described as follows:

$$R_a = \frac{1}{l} \int_0^l |z(x)| dx \tag{Eq 1}$$

$$R_q = \sqrt{\frac{1}{l} \int_0^l z^2(x) dx} \tag{Eq 2}$$

$$S_k = \frac{1}{l} \int_0^l \frac{z^3(x)}{R_q^3} dx, \tag{Eq 3}$$

where l is the measuring distance, and $z(x)$ is the surface height.

At relatively low preheating temperatures (below 200 °C), all these three parameters did not change significantly.

The surface composition changes at different preheating temperatures are summarized in Table 3. The data in Table 3 did not represent the compositions of the bulk material because XPS analysis could only detect the composition of a very small surface area with the maximum depth of around 10 nm. To investigate the change of surface moisture with preheating temperature, the narrow-scan oxygen profile was resolved into three binding energies—530.2, 531.9, and 533.2 eV—which represent oxide, hydroxide, and physically adsorbed moisture (Ref 18). Figure 4 shows the results of the oxygen peak fitting and the relative atom percent of oxide, hydroxide, and moisture. The ratios of hydroxide/oxide and moisture/oxide decreased dramatically as the substrate preheating temperatures increased.

As shown in Fig. 4, at elevated temperatures, the metal oxide component increased due to thermal oxidation while the hydroxides (chemically adsorbed) and moisture (physically adsorbed) decreased. For substrates heated to 150 °C, the moisture was efficiently removed. Whereas a certain degree of hydroxides were still present on the substrate surface (even at 200 °C), they could dehydrate into gas vapor during hot droplet spreading and be the source for the pore formation. The amount of carbon present on the substrate surface decreased greatly with the increasing temperature as adventitious carbon was oxidized and released to the environment. At the same time, the surfaces became enriched in Fe and O, and relatively depleted in Cr. It should be noted that the surface composition changes when the stainless steel substrates undergo thermal treatment to remove surface moisture.

3.3 Splat Morphology Characterization

To characterize in detail the transition behavior of splats, splats were categorized into four typical geometries, shown in Fig. 5. The extent of splashing decreased on progression from type 1 to type 4. This classification is consistent with our previous studies (Ref 19). Type 1 splats had small cooling rates which induced droplet overspreading and fragmentation. Therefore, type 1 splats only had a central core and a solid ring surrounding it. Because of the increased cooling rates compared with type 1 splats, type 2 splats showed a less extent of splashing with more materials remaining on the substrate. Generally, the central core of type 1 and 2 splats adhered well with the substrate, while most materials of type 3 and 4 splats showed excellent contact with the substrate. Compared to type 1 splats, improved contact and faster solidification reduced the fragmentation of type 2 splats. In this study, at lower substrate temperatures of RT and 100 °C, highly splashed splats mainly consisted of type 1 and type 2. While on hotter substrates, a proportion of droplet material projected out from the periphery, forming the splashed fingers, seen type 3. Type 4 splats were perfect disk shapes with no material extending from the central core.

To characterize the spreading behavior of splats on different preheated substrates, three ratios were measured. Here, the overall flattening ratio ξ_f is defined as the ratio of the overall splat diameter (D_r for type 1 and type 2 splats, D_d for the rest) to the original average particle size ($D_0 = 54$ μm). Mostly, for type 2 splats, there was also an obvious solid ring (diameter D_r) surrounding the central core. Even though the diameter of this ring was smaller than that of the finger tips, these finger tips seemed like ejecting away from this solid ring probably due to the instability induced by fast solidification. When the spreading diameter of type 2 splats was measured, this remaining ring was carefully recognized and located to avoid random choice. The central flat area ratio ξ_c is defined as the ratio of the central flat area diameter (D_c) to the overall splat diameter (D_r or D_d). The flattening ratio of the central flat area ξ_c is determined by the ratio of D_c to D_0. As seen in Fig. 5(d), the central smooth area was thinner compared with the rim part which experiences curling-up due to droplet recoiling and cooling stress (Ref 20, 21). Notably, no disordered oscillation, named
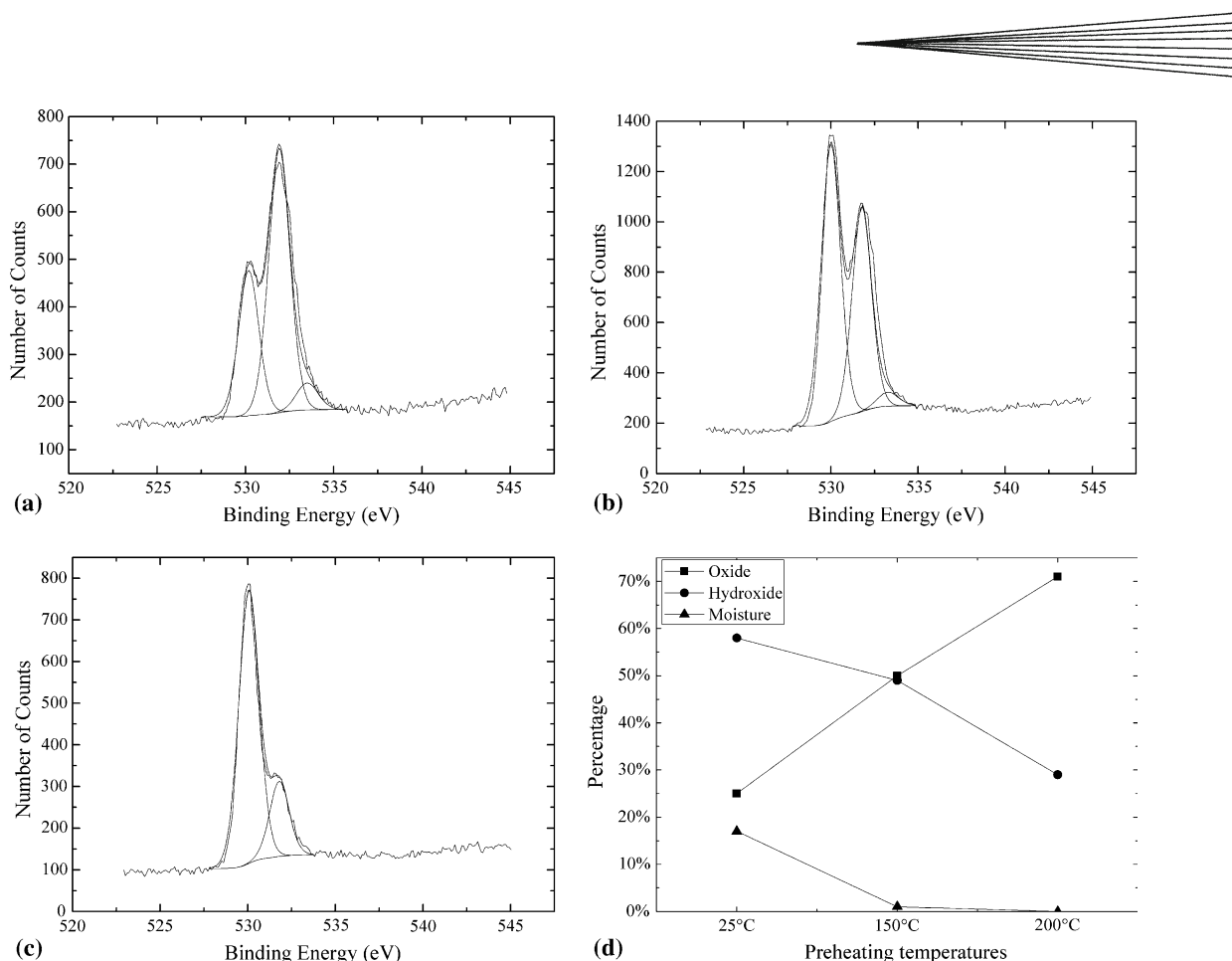
Fig. 4 Oxygen profiles on the substrate surface at different heating temperatures (a) room temperature, (b) 150 °C, (c) 200 °C, and (d) percentage changes

water-wave pattern, can be observed for the central flat area.

Frequently, some small size splats were observed (Fig. 5c and d). During molten droplet spreading, some molten materials could jet away from the spreading surface (Ref 22), which solidified into small disk splats afterwards. Meanwhile, the irregular particles and small nodules shown in Fig. 1 may break up during flight, generating smaller size droplets and smaller splat diameters accordingly. Nevertheless, the formation mechanism of these small size splats still remains unclear. It is necessary to determine the cut-off diameter for the primary impacting and spreading splats, in order to accurately compare the flattening ratios of these two powder materials. Hence, around 500 splats of Ni and Ni20Cr (including the small size splats) at 200 °C were utilized as an example to determine a suitable cut-off diameter representing the primary spreading splats. The distribution of splat diameters is shown in Fig. 6. The splats with small spreading diameters, below 60 μm, occupied the majority by number. Above that, the splat diameters showed a bimodal distribution with two possible thresholds, 90 or

150 μm. In order to confirm the final diameter threshold, one could assume that all the materials of an original spherical particle totally transform into a cylinder splat. So the mass conservation can be expressed by

$$\rho \frac{4}{3}\pi \left(\frac{D_0}{2}\right)^3 = \rho\pi \left(\frac{D_d}{2}\right)^2 \delta, \tag{Eq 4}$$

where δ represents the thickness of one splat and ρ is the particle density.

For one original particle with a size of 40 μm, the calculated splat diameter is 146.1 μm with a thickness of 2 μm, which is a typical thickness of splats formed on the heated substrates (Ref 3). Therefore, for type 3 and 4 splats of Ni and Ni20Cr, only the splats with diameters bigger than 145 μm were evaluated. However, for type 1 and 2 splats, it was difficult to characterize the maximum spreading diameter and the exact location where the droplet began disintegrating from the final splat morphology. Hence, the diameter 145 μm was also used as the cut-off size to eliminate too small splats. But more work will be conducted to develop a robust method to confirm the cut-off diameter for type 1 and 2 splats.
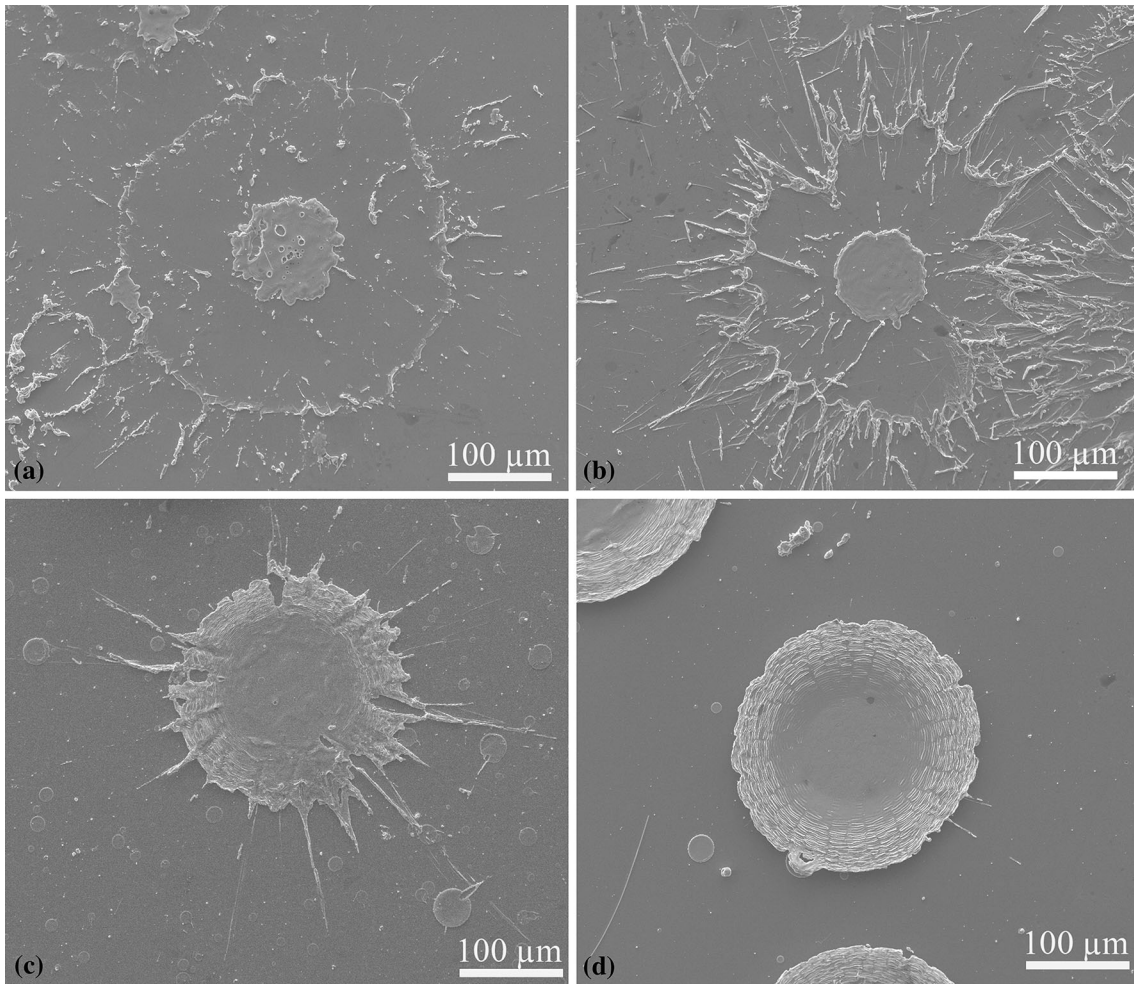
Fig. 5 Different categories of splat morphologies (a) type 1 halo splat, (b) type 2 fingered halo splat, (c) type 3 fingered disk splat, (d) type 4 perfect disk splat
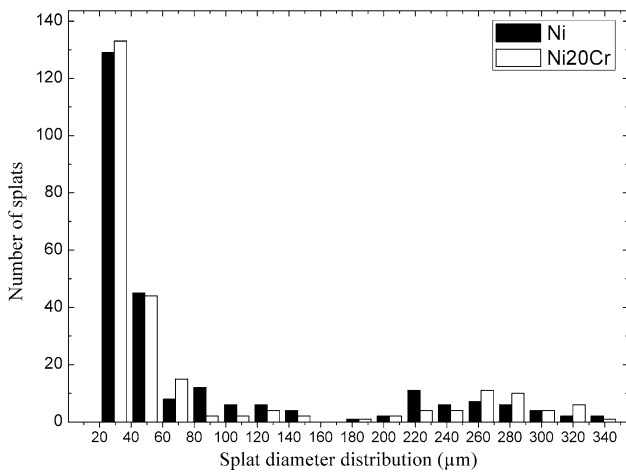

Fig. 6 The diameter distribution of Ni and Ni20Cr splats

3.4 Transitional Change of the Splat Morphology

As the substrate temperature increases, the regular shaped splats without fragmentation are formed, i.e., there is a transitional change of splat shapes. Figure 7 describes the percentage of different types of splats found on the substrates. For Ni splats of Fig. 7(a), at room temperature, all the splats showed type 1. When the substrate was heated to 100 °C, the number of type 1 splats dramatically decreased to 8% and type 2 splats increased to 92% (Fig. 7a). This suggests that there was improved contact between the splat and the substrate. At 125 °C, the proportion of type 2 splats reduced to 18% and type 3 splats dominated, occupying 82%. Even though the rapid droplet solidification dissipates part of inertial energy, the upper liquid still had enough kinetic energy to overcome viscosity and surface tension, generating splashed fingers. Therefore, as the substrate heating temperature increased to 150 °C, splats were completely composed of type 3 splats, while type 2 splats induced by material overspreading were absent. Above 150 °C, the proportion of
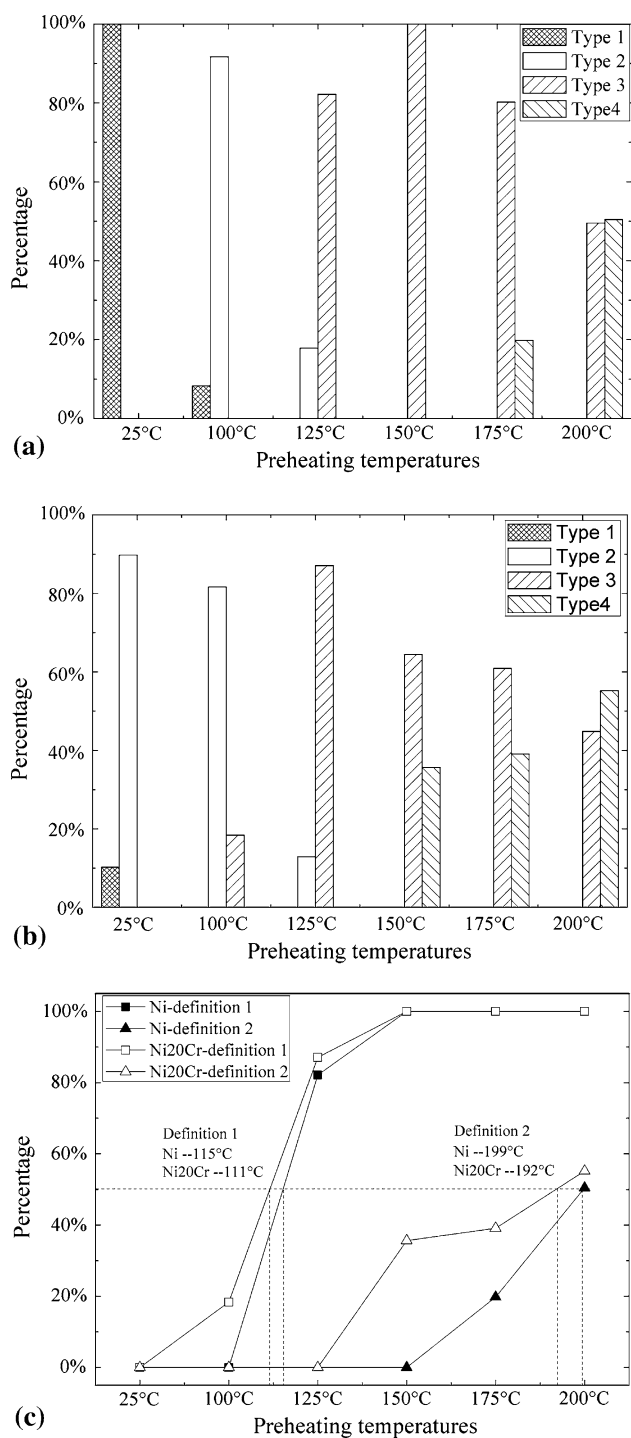
(a)

(b)

(c)

Fig. 7 The fraction of different types of splats with respect to different preheating temperatures (a) Ni splats, (b) Ni20Cr splats and (c) transition temperatures characterization

disk splats increased but did not dominate, only ~50% of splats showing perfect disk shapes without any splashing. Preheating substrates to 150 °C and above effectively eliminated extensive material projections and ensured the formation of regular disk-type splats.

The population of Ni20Cr splats is summarized in Fig. 7(b). On the substrates at room temperature, type 2 splats comprised the majority nearly 90%. Compared with Ni splats only showing type 1 splats, the addition of Cr promoted more material of the droplet adhering with substrate. After the substrate was heated to 100 °C, no type 1 splats were formed. However, type 3 splats were observed (18%); this also suggested that introducing element Cr could reduce splashing perhaps through improving droplet wettability. Above 150 °C, type 2 splats also disappeared. This trend was similar to that of Ni splats, indicating a similar splat formation mechanism among them. One should note that for Ni20Cr powder, the formation of type 3 splats was greatly restrained at 150 °C, dropping from 100% of Ni splats to ~64% of Ni20Cr splats. In addition, the perfect disk splats of Ni20Cr emerged at 150 °C, while the same phenomenon was observed on substrates heated above 175 °C for Ni splats.

Furthermore, the estimation of transition temperature is strongly dependent on the definition of a disk splat. In this study, type 3 and 4 splats showed predominantly disk shapes with different splashing degrees, while type 1 and 2 were extensively splashed splats. Therefore, a disk splat could justifiably be defined as either all of type 3 and 4 (definition 1), or type 4 only (definition 2, where splashing was minimal or non-extent). The former is more consistent with the definition used by Fukumoto et al. (Ref 2). Figure 7(c) plots the transition temperature using both of these two definitions, for Ni and Ni20Cr splats. There was a significant difference in the transition temperature depending on the definition used. For example, for Ni splats, the transition temperature changed from 115 °C (definition 1) to 199 °C (definition 2). However, regardless of the definition of disk splats, the addition of Cr made no significant difference to the transition temperature. The small difference of transition temperatures between Ni and Ni20Cr splats is different from Fukumoto's observation where Ni20Cr powder (106 °C) has a much smaller transition temperature than Ni powder (273 and 337 °C) reported in Ref 2. The transition temperatures of Ni and Ni20Cr splats were around the temperature, 150 °C, where most moisture was removed. It is difficult to characterize the effect of alloying elements on the evolution of splat formation by only considering the parameter of transition temperature. But indeed, the addition of element Cr changed the splat formation, which can be observed from the fraction changes of different types of splats.

3.5 Splat Diameters as the Function of Preheating Temperatures

Figure 8(a), (c) and (e) illustrates the flattening behavior of Ni splats. For type 2 splats, even though the liquid fragmentation occurred after maximum spreading, the streaks surrounding the central core depicted the spreading trajectory of splats, without much recoiling. Therefore, under the same heating conditions, these splats always showed the largest flattening ratios (Fig. 8a). While for type 1 splats, the liquid part of the droplet could break
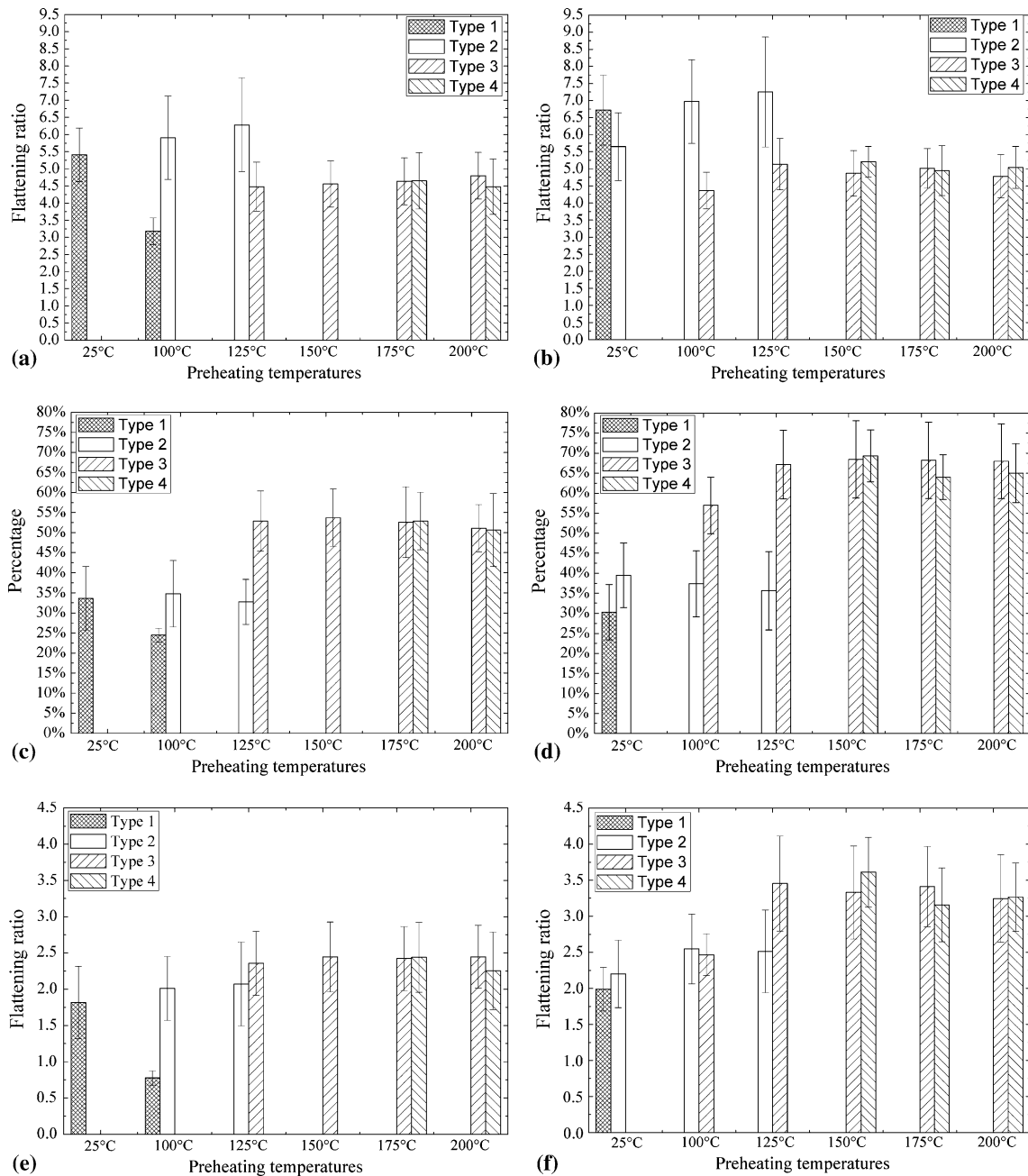
Fig. 8 Morphology information of Ni splats (a) overall flattening ratios ξ_f, (b) ξ_f, (c) central flat area ratios ξ_c, (d) ξ_c, (e) flattening ratio of the central flat area ζ_c, and Ni20Cr splats (f) ζ_c

up either from the holes initially formed inside the splat during spreading or around the splat rim (Ref 23, 24). Therefore, the diameter of residual rings may not represent the maximum spreading. They showed smaller flattening ratios compared with type 2 splats. It was observed that in the formation of regular disk splats (type 3 and 4), the overall flattening ratios were quite similar despite the different preheating temperatures. The spreading behavior of the central smooth area is shown in Fig. 8(c) and (e). Generally, during droplet spreading, this central area

contacts closely with the substrate because of the high impact pressure (Ref 25). Above 150 °C, once most of the moisture was removed, the central flat area occupied similar ratios of the whole splat area (type 3 and 4), around 45-60% (Fig. 8c). The high impact pressure of the droplet could only effectively generate good interfacial contact within $\xi_f < 2$, overcoming the upward force induced by the vaporized moisture from the substrate surface (Ref 25). It can be observed that due to the existence of surface moisture, the flattening ratio of the central flat
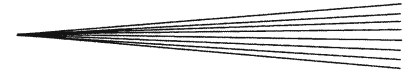
area was about $\zeta_c \sim 2$ on substrates below 150 °C (Fig. 8e).

Figure 8(b), (d), and (f) depicts the flattening behavior of Ni20Cr splats. At room temperature, the flattening ratio of type 1 splats (Fig. 8b) was slightly larger than that of Ni splats. Due to the improved adhesion of Ni20Cr splats on the substrate, the reach of the residual rings could be maintained close to the furthest spreading point regardless of liquid breakup inside the splat. For type 2 splats, similar to Ni splats, they showed the largest flattening ratios. It should be noticed that like the observation of Ni splats, the flattening ratios of Ni20Cr splats on substrates heated above 150 °C were also similar and only slightly increased to 4.5-6 from 4 to 5.5 of Ni splats. Figure 8(d) and (f) presents the ratios ξ_c and ζ_c of the central flat area for Ni20Cr splats. In the spreading process of disk-shaped splats (type 3 and 4), the ratio ξ_c of Ni20Cr splats (Fig. 8d) was much bigger than Ni splats, increasing from 45-60% of Ni to 60-80% of Ni20Cr. When the moisture was present on the substrate surface, the ratio ζ_c of Ni20Cr spats was kept similar (Fig. 8f), but it slightly increased compared to the Ni splats.

4. Discussion

4.1 Effect of Substrate Surface Conditions on Splat Formation

When the substrates were heated to relatively low temperatures below 200 °C, the surface topology did not change significantly, meaning that surface roughness unlikely to be the cause of different spreading behavior. Accordingly, the changes of friction and wettability induced by the surface roughness are assumed to be negligible. The transition from highly splashed (type 1 and 2) to disk-like splats (types 3 and 4) correlated with the removal of a significant proportion of surface moisture and surface hydroxides as observed in the XPS analysis. On substrates heated below 150 °C, lots of surface moisture and hydroxides adhere on the surface. During the hot droplet spreading, the moisture and hydroxides are released to form a gas layer along the splat-substrate interface, inhibiting the interfacial contact and heat transfer. Accordingly, the droplets stay in the liquid form for a longer time and flatten to a larger extent. Then the droplets could break up due to the over-spreading of the liquid part, inducing the formation of type 1 and 2 splats and their larger flattening ratios. As preheating temperatures increased, moisture adhering to substrate surface was efficiently removed, reducing from 17% at RT to less 1% at 150 °C. The hydroxide content also reduced from 58% at RT to 29% at 200 °C. Therefore, the significant reduction of fragmented splats (type 1 and 2) is the result of the removal of surface moisture and hydroxides along the splat-substrate interface because of the thermal treatment. But meanwhile, the existence of surface hydroxides (49% at 175 °C and 29% at 200 °C) could probably induce the formation of finger projections above 150 °C, because these hydroxides could decompose into

oxides and release gas vapor (Ref 26). Interestingly, when the moisture and hydroxides are being removed from substrate surface, the ratio of Fe/Cr is also changing and may play a role in the formation of splashed fingers. Considering that the surface roughness was kept consistent under these conditions, the formation of splat splashing on 304 stainless steel substrates is not solely dependent on the removal of moisture, but also on the surface composition. Although a certain degree of hydroxides existing on the substrate surface could lead to the formation of type 3 splashed splats, the surface composition changes during preheating cannot be neglected to make a contribution. Therefore, in the future, it is necessary to eliminate the great changes of surface composition to investigate splat formation mechanism. When less gas is vaporized, the better contact between the droplet and substrate is achieved and thus faster cooling rates of the droplets. Consequently in the formation of disk splats, similar flattening ratios of type 3 and 4 splats are observed for each powder material.

4.2 The Effect of Alloying Element Cr on Splat Formation

When moisture exists along the droplet-substrate interface, droplet fragmentation or significant splashing may occur. However, more materials of Ni20Cr splats could still remain on the substrate surface, showing a better adhesion condition compared to the Ni splats. After moisture vaporized, for Ni20Cr splats, the ratios ξ_c of type 3 and 4 splats became larger than that of Ni splats. In addition, the area that the central flat portion of Ni20Cr splats covered was also wider than that of Ni splats, indicating that during droplet spreading, less material detached from the substrates. More microstructure analysis along the splat-substrate interface is needed. Similar to Ni splats, the central core of disintegrated Ni20Cr splats (type 1 and 2) achieved the flattening ratio of ~2. It appears that the impact pressure of the droplet plays an important role in determining the spreading behavior of the central smooth area. However, with the decline of impact pressure around the periphery, the competition of surface tension, wettability, and viscosity of the droplets may become dominant in forming the oscillating structure.

Goutier et al. suggested that the surface tension of the molten droplet played an important role in the droplet flattening ratio (Ref 12). The high temperature properties of the coating materials such as surface tension and viscosity are summarized in Table 4. These two coating materials have similar melting point, density, and viscosity, while the surface tension of Ni20Cr droplets is smaller than Ni droplets. In this study, Ni and Ni20Cr powders were sprayed using the same spraying parameters. So it is supposed they had similar velocity and temperature profiles upon impact. It has been pointed out that when the thermal conductivity of plasma-sprayed oxide particles increases, the corresponding transition temperatures decrease (Ref 11). However, in our case of sprayed metallic particles, the transition temperatures show little difference even though Ni has a larger thermal conductivity. The

Table 4 High temperature properties of sprayed powders at melting points

	Ni	Ni20Cr
Surface tension, mN/m	1800 (Ref 29)	1350 (Ref 30)
Viscosity, mPa s	6 (Ref 29)	5.8 (Ref 31)
Density, g/m^3	7820 (Ref 31)	7410 (Ref 31)
Melting point, K	1728 (Ref 31)	1700 (Ref 31)
Thermal conductivity, W/m/K	69 (Ref 32)	37 (Ref 33)
Thermal diffusivity, 10^6 m^2/s	12 (Ref 32)	5 (Ref 33)

difference in thermal conductivities and thermal diffusivities of particles may make a contribution to the cooling rates which, however, are mainly controlled by the heat transfer coefficient along droplet-substrate interface (Ref 27, 28).

Based on this assumption, the changed spreading behavior of Ni20Cr splats was related to the addition of element Cr, because of the reduced surface tension (seen in Table 4). The surface tension is regarded as the resistant force during droplet spreading and the driving force during droplet recoiling. Therefore, a smaller surface tension could facilitate droplet spreading and generate a bigger splat diameter. The peripheral oscillating is restrained somehow and more smooth area is formed for Ni20Cr splats. Meanwhile, a smaller surface tension of Ni20Cr, representing a smaller surface energy of the liquid alloy, could generate a lower contact angle from the Young's equation,

$$\cos \theta = \frac{\sigma_{SV} - \sigma_{SV}}{\sigma_{SV}}, \qquad (Eq\ 5)$$

where θ stands for the contact angle, σ_{SV} is the solid surface energy, σ_{LV} is the liquid surface energy, and σ_{SL} is the solid/liquid interfacial energy. It is supposed that the improved wettability of Ni20Cr optimizes the droplet spreading behavior and promotes more perfect disk splats (type 4).

5. Conclusions

In order to investigate the effects of alloyed element Cr of coating materials on splat spreading, sieved Ni and Ni20Cr powders were plasma sprayed onto stainless steel preheated to different temperatures. The splat morphologies were systematically analyzed.

The results show that the surface roughness of 304 stainless steel substrates held at temperatures below 200 °C was kept consistent. The moisture and hydroxides present on the substrate surface caused splat fragmentation and over-spreading, resulting into the largest flattening ratio. After moisture was removed through preheating substrates above 150 °C, the overall flattening ratios and central flat area ratios were kept consistent for the same coating material. However, the surface composition change could also play a role in causing a certain degree of droplet dewetting during the formation of disk splats. It is easier for Ni20Cr splats undergoing the transition from

splashing splats to disk ones. Nevertheless, Ni and Ni20Cr splats show similar transition temperatures which also depends on the definitions of disk shape splats. Besides, during the formation of Ni20Cr disk splats, a larger central flat area ratio can be achieved, due to the small surface tension. Therefore, after adding active element Cr, the contact angles of droplets may be reduced and thus the improved wettability during spreading, facilitating the splats contacting with the substrate.

References

1. M. Fukumoto and Y. Huang, Flattening Mechanism in Thermal Sprayed Nickel Particle Impinging on Flat Substrate Surface, *J. Therm. Spray Technol.*, 1999, **8**(3), p 427-432
2. M. Fukumoto, T. Yamaguchi, M. Yamada, and T. Yasui, Splash Splat to Disk Splat Transition Behavior in Plasma-Sprayed Metallic Materials, *J. Therm. Spray Technol.*, 2007, **16**(5-6), p 905-912
3. S. Brossard, P.R. Munroe, A.T. Tran, and M.M. Hyland, Study of the Splat Microstructure and the Effects of Substrate Heating on the Splat Formation for Ni-Cr Particles Plasma Sprayed onto Stainless Steel Substrates, *J. Therm. Spray Technol.*, 2010, **19**(5), p 1100-1114
4. V. Pershin, M. Lufitha, S. Chandra, and J. Mostaghimi, Effect of Substrate Temperature on Adhesion Strength of Plasma-Sprayed Nickel Coatings, *J. Therm. Spray Technol.*, 2003, **12**(3), p 370-376
5. X. Jiang, Y. Wan, H. Herman, and S. Sampath, Role of Condensates and Adsorbates on Substrate Surface on Fragmentation of Impinging Molten Droplets During Thermal Spray, *Thin Solid Films*, 2001, **385**(1), p 132-141
6. A.T.T. Tran, M.M. Hyland, T. Qiu, B. Withy, and B.J. James, Effects of Surface Chemistry on Splat Formation During Plasma Spraying, *J. Therm. Spray Technol.*, 2008, **17**(5-6), p 637-645
7. A. McDonald, M. Lamontagne, C. Moreau, and S. Chandra, Impact of Plasma-Sprayed Metal Particles on Hot and Cold Glass Surfaces, *Thin Solid Films*, 2006, **514**(1), p 212-222
8. C.-J. Li and J.-L. Li, Evaporated-Gas-Induced Splashing Model for Splat Formation During Plasma Spraying, *Surf. Coat. Technol.*, 2004, **184**(1), p 13-23
9. J. Cedelle, M. Vardelle, and P. Fauchais, Influence of Stainless Steel Substrate Preheating on Surface Topography and on Millimeter-and Micrometer-Sized Splat Formation, *Surf. Coat. Technol.*, 2006, **201**(3), p 1373-1382
10. M. Fukumoto, H. Nagai, and T. Yasui, Influence of Surface Character Change of Substrate Due to Heating on Flattening Behavior of Thermal Sprayed Particles, *J. Therm. Spray Technol.*, 2006, **15**(4), p 759-764
11. P. Fauchais, A. Vardelle, M. Vardelle, and M. Fukumoto, Knowledge Concerning Splat Formation: An Invited Review, *J. Therm. Spray Technol.*, 2004, **13**(3), p 337-360
12. K. Yang, M. Fukumoto, T. Yasui, and M. Yamada, Role of Substrate Temperature on Microstructure Formation in Plasma-Sprayed Splats, *Surf. Coat. Technol.*, 2013, **214**, p 138-143
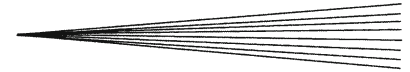
13. J.X. Zhang, R.S. Chandel, and H.P. Seow, Effects of Chromium on the Interface and Bond Strength of Metal-Ceramic Joints, *Mater. Chem. Phys.*, 2002, **75**(1), p 256-259

14. K. Nakashima, H. Matsumoto, and K. Mori, Effect of Additional Elements Ni and Cr on Wetting Characteristics of Liquid Cu on Zirconia Ceramics, *Acta Mater.*, 2000, **48**(18), p 4677-4681

15. P. Kritsalis, V. Merlin, L. Coudurier, and N. Eustathopoulos, Effect of Cr on Interfacial Interaction and Wetting Mechanisms in Ni Alloy/Alumina Systems, *Acta Metall. Mater.*, 1992, **40**(6), p 1167-1175

16. G.-J. Yang, C.-X. Li, S. Hao, Y.-Z. Xing, E.-J. Yang, and C.-J. Li, Critical Bonding Temperature for the Splat Bonding Formation During Plasma Spraying of Ceramic Materials, *Surf. Coat. Technol.*, 2013, **235**, p 841-847

17. C.-J. Li, H.-L. Liao, P. Gougeon, G. Montavon, and C. Coddet, Experimental Determination of the Relationship Between Flattening Degree and Reynolds Number for Spray Molten Droplets, *Surf. Coat. Technol.*, 2005, **191**(2), p 375-383

18. C.-C. Shih, C.-M. Shih, Y.-Y. Su, L.H.J. Su, M.-S. Chang, and S.-J. Lin, Effect of Surface Oxide Properties on Corrosion Resistance of 316L Stainless Steel for Biomedical Applications, *Corros. Sci.*, 2004, **46**(2), p 427-441

19. A.T.T. Tran, M.M. Hyland, K. Shinoda, and S. Sampath, Influence of Substrate Surface Conditions on the Deposition and Spreading of Molten Droplets, *Thin Solid Films*, 2011, **519**(8), p 2445-2456

20. S. Goutier, M. Vardelle, and P. Fauchais, Comparison Between Metallic and Ceramic Splats: Influence of Viscosity and Kinetic Energy on the Particle Flattening, *Surf. Coat. Technol.*, 2013, **235**, p 657-668

21. G. Bolelli, K. Sabiruddin, L. Lusvarghi, E. Gualtieri, S. Valeri, and P.P. Bandyopadhyay, FIB Assisted Study of Plasma Sprayed Splat-Substrate Interfaces: NiAl-Stainless Steel and Alumina-NiAl Combinations, *Surf. Coat. Technol.*, 2010, **205**(2), p 363-371

22. C. Le Bot, S. Vincent, E. Meillot, F. Sarret, J.-P. Caltagirone, and L. Bianchi, Numerical Simulation of Several Impacting Ceramic Droplets with Liquid/Solid Phase Change, *Surf. Coat. Technol.*, 2014, **268**, p 272-277

23. A. Vardelle, C. Moreau, N.J. Themelis, and C. Chazelas, A Perspective on Plasma Spray Technology, *Plasma Chem. Plasma Process.*, 2015, **35**(3), p 491-509

24. N.Z. Mehdizadeh, M. Lamontagne, C. Moreau, S. Chandra, and J. Mostaghimi, Photographing Impact of Molten Molybdenum Particles in a Plasma Spray, *J. Therm. Spray Technol.*, 2005, **14**(3), p 354-361

25. C.-J. Li and J.-L. Li, Transient Contact Pressure During Flattening of Thermal Spray Droplet and Its Effect on Splat Formation, *J. Therm. Spray Technol.*, 2004, **13**(2), p 229-238

26. A.T.T. Tran, M.M. Hyland, K. Shinoda, and S. Sampath, Inhibition of Molten Droplet Deposition by Substrate Surface Hydroxides, *Surf. Coat. Technol.*, 2011, **206**(6), p 1283-1292

27. M. Pasandideh-Fard, V. Pershin, S. Chandra, and J. Mostaghimi, Splat Shapes in a Thermal Spray Coating Process: Simulations and Experiments, *J. Therm. Spray Technol.*, 2002, **11**(2), p 206-217

28. M. Vardelle, A. Vardelle, A.C. Leger, P. Fauchais, and D. Gobin, Influence of Particle Parameters at Impact on Splat Formation and Solidification in Plasma Spraying Processes, *J. Therm. Spray Technol.*, 1995, **4**(1), p 50-58

29. S. Mukherjee, W.L. Johnson, and W.K. Rhim, Noncontact Measurement of High-Temperature Surface Tension and Viscosity of Bulk Metallic Glass-Forming Alloys Using the Drop Oscillation Technique, *Appl. Phys. Lett.*, 2005, **86**(1), p 014104

30. F. Xiao, R. Yang, and C. Zhang, Surface Tension of Molten Ni-W and Ni-Cr Alloys, *Mater. Sci. Eng. B*, 2006, **132**(1), p 183-186

31. H. Kobatake and J. Brillo, Density and Viscosity of Ternary Cr-Fe-Ni Liquid Alloys, *J. Mater. Sci.*, 2013, **48**(19), p 6818-6824

32. K.C. Mills, *Recommended Values of Thermophysical Properties for Selected Commercial Alloys*, Woodhead Publishing, Cambridge, 2002

33. Y.V. Glagoleva, N.B. Pushkareva, Y.E. Lapshova, O.V. Sadyreva, V.F. Polev, V.I. Gorbatov, S.G. Taluts, and I.G. Korshunov, Thermophysical and Transport Properties of Nickel-Chromium Alloys at High Temperatures, *Phys. Met. Metallogr.*, 2006, **102**(1), p 48-54